18th International Conference on Information Fusion
Washington, DC - July 6-9, 2015

Accuracy and Consistency in Estimation and Fusion over Long-Haul Sensor Networks

Qiang Liu
Department of Electrical and Computer Engineering
Stony Brook University
Stony Brook, NY 11794–2350
Email: qiangliu@ece.sunysb.edu

Xin Wang
Department of Electrical and Computer Engineering
Stony Brook University
Stony Brook, NY 11794–2350
Email: xwang@ece.sunysb.edu

Nageswara S. V. Rao
Oak Ridge National Laboratory
Oak Ridge, TN 37831-6355
Email: raons@ornl.gov

***Abstract*—Long-haul sensor networks can be found in many real-world applications, such as tracking and/or monitoring of one or more dynamic targets in space. In such networks, sensors are remotely deployed over a large geographical area, whereas a remote fusion center fuses the information provided by these sensors in order to improve the accuracy of the final estimates of certain target characteristics. We consider the accuracy as well as consistency of information measures such as the error covariance matrices used to describe the theoretical error performance of sensor and fuser estimates. In particular, the impact of filtering and fusion, communication loss and delay, sensor bias, and information feedback on the accuracy and consistency of error measures is investigated by means of studying a maneuvering target tracking application.**

***Index Terms*—Long-haul sensor networks, state estimate fusion, error covariance matrices, estimation bias, information consistency, information feedback, root-mean-square-error (RMSE) performance, reporting deadline.**

I. INTRODUCTION

In long-haul sensor networks, sensors with sensing, data processing, and communication capabilities are deployed to cover a very large geographical area, such as a continent or even the entire globe, and are tasked for applications such as target tracking and monitoring. A remote sensor measures certain parameters of interest from the dynamic target(s) on its own, and then sends the state estimates it derives from these measurements to the fusion center. The fusion center serves to collect data from multiple such sensors and fuse these data to obtain global estimates periodically at specified time instants.

There exist many challenges in estimation and fusion over such long-haul connections. The signal propagation time can be significant, due to the long distances, in the tens of thousands of miles for satellite links, for instance. Communication is often subject to sporadic high bit-error rates (BERs) and burst losses that can effectively reduce the number of reliable estimates available at the fusion center. As a result, the global estimates may not be promptly and accurately finalized by the fusion center, leading to degraded fusion performance and even failures to comply with the system requirements on the worst-case estimation error and/or maximum reporting delay, both crucial elements for near real-time performance in many applications. Some sensors may also be prone to estimation bias, as a result of poor calibration or environmental factors.

In the literature, some works have attempted to address estimation and/or fusion under variable communication loss and/or delay conditions. In [2] and [11], estimation and fusion performances using Kalman filters (KFs) under variable packet loss rates have been studied. [8] and [15] have addressed filtering in the context of out-of-sequence measurements (OOSMs), where all data would finally arrive despite the random delay. [7] and [10] have exploited retransmission to recover some of the lost messages over time so that the effect of information loss can be somewhat mitigated. More recently, a staggered estimation scheduling scheme and an information feedback mechanism have been proposed in [4] and [5] respectively that aim to improve the overall tracking performance by exploring the relationships of sensor data over time and sensor-fuser data across space.

A number of data fusion methods have been developed over the years, with a primary goal of taking in the data from multiple sensors – which typically output and communicate their own state estimates and the corresponding error covariances – and combining them to produce a condensed set of meaningful information (state estimates and error covariances as well) with the highest possible degree of accuracy and certainty [1]. A question then arises of how well the error covariance matrices – as theoretical measurements of the error performance – could describe the actual estimation error level of the corresponding state estimates; in other words, if the two are consistent. Besides investigating the accuracy performance, this work also aims to answer the above question by exploring the consistency of error covariances under a number of conditions, including target motion uncertainty, filter and fuser types, communication loss and delay, sensor bias, and information feedback, among others. A maneuvering target tracking example is used throughout to demonstrate the performance of tracking accuracy and information consistency.

The remainder of this paper is organized as follows: The system model is outlined in Sec. II. In Secs. III and IV, we explore the estimation and consistency performances using one sensor, and a combination of two sensors, respectively, under variable conditions. The effect of information feedback is investigated in Sec. V via analytical and simulation studies. The paper concludes in Sec. VI.

II. System Model

In this section we present the target and sensor measurement models as well as the estimation and fusion algorithms.

A. Target Model

We consider a trajectory that consists of two basic types of motion: straight-line and turn movements, which are described by the continuous white-noise acceleration (CWNA) and coordinated turn (CT) models respectively.

1) Continuous White-Noise Acceleration (CWNA) Model: The discretized CWNA model is a simple, commonly used motion model in which an object moving in a generic coordinate ξ is assumed to be traveling at a near constant speed. The discrete-time state equation is given by $\mathbf{x}_{k+1} = \mathbf{F}\mathbf{x}_k + \mathbf{w}_k$, where (dropping the time index k), $\mathbf{x} = [\xi \quad \dot{\xi}]^T$ here is a vector representing the position and velocity, and $\mathbf{F}$ is known as the transition matrix and is given by $\mathbf{F} = \begin{bmatrix} 1 & T \\ 0 & 1 \end{bmatrix}$, where T is the scan rate of the sensor[1] (i.e., sampling period). The covariance of the discrete-time process noise $\mathbf{w}_k$ is $\mathbf{Q} = \tilde{q}\begin{bmatrix} T^3/3 & T^2/2 \\ T^2/2 & T \end{bmatrix}$, where $\tilde{q}$ (often assumed to be constant over time) is the power spectral density (PSD) of the underlying continuous-time white stochastic process.

In many scenarios, the motion along each coordinate (such as in the "east-north-up" coordinate system [1]) is typically assumed to be decoupled from the other coordinates; as such, the same model is used for each coordinate. Since our focus is on 2-D tracking, we extend the above model to two coordinates ξ and η. The evolution of the state vector $\mathbf{x} = [\xi \quad \dot{\xi} \quad \eta \quad \dot{\eta}]^T$ is described by

$$\mathbf{x}_{k+1} = \begin{bmatrix} \begin{bmatrix} 1 & T \\ 0 & 1 \end{bmatrix} & \mathbf{0}_{2\times 2} \\ \mathbf{0}_{2\times 2} & \begin{bmatrix} 1 & T \\ 0 & 1 \end{bmatrix} \end{bmatrix} \mathbf{x}_k + \mathbf{w}_k, \tag{1}$$

and the covariance matrix $\mathbf{Q}_k$ of the process noise $\mathbf{w}_k$ is

$$\mathbf{Q}_k = \begin{bmatrix} \tilde{q}_\xi \begin{bmatrix} T^3/3 & T^2/2 \\ T^2/2 & T \end{bmatrix} & \mathbf{0}_{2\times 2} \\ \mathbf{0}_{2\times 2} & \tilde{q}_\eta \begin{bmatrix} T^3/3 & T^2/2 \\ T^2/2 & T \end{bmatrix} \end{bmatrix}. \tag{2}$$

2) Target Maneuver: The second type of motion occurs when the target performs a maneuver (i.e., a turn). A turn usually follows a pattern known as a *coordinated turn*, which is characterized by a constant turn rate and a constant speed. The turn rate Ω is incorporated into the motion model by augmenting the state vector for a horizontal motion model: $\mathbf{x} = \begin{bmatrix} \xi & \dot{\xi} & \eta & \dot{\eta} & \Omega \end{bmatrix}^T$, which gives rise to the discretized coordinated turn (CT) model [1], given by

$$\mathbf{x}_{k+1} = \begin{bmatrix} 1 & \frac{\sin\Omega(k)T}{\Omega(k)} & 0 & -\frac{1-\cos\Omega(k)T}{\Omega(k)} & 0 \\ 0 & \cos\Omega(k)T & 0 & -\sin\Omega(k)T & 0 \\ 0 & \frac{1-\cos\Omega(k)T}{\Omega(k)} & 1 & \frac{\sin\Omega(k)T}{\Omega(k)} & 0 \\ 0 & \sin\Omega(k)T & 0 & \cos\Omega(k)T & 0 \\ 0 & 0 & 0 & 0 & 1 \end{bmatrix} \mathbf{x}_k + \mathbf{w}_k, \tag{3}$$

where $\mathbf{w}_k$ is the process noise whose covariance matrix is given by

$$\mathbf{Q}_k = \begin{bmatrix} \tilde{q}_\xi \begin{bmatrix} T^3/3 & T^2/2 \\ T^2/2 & T \end{bmatrix} & \mathbf{0}_{2\times 2} & \begin{matrix} 0 \\ 0 \end{matrix} \\ \mathbf{0}_{2\times 2} & \tilde{q}_\eta \begin{bmatrix} T^3/3 & T^2/2 \\ T^2/2 & T \end{bmatrix} & \begin{matrix} 0 \\ 0 \end{matrix} \\ \begin{matrix} 0 & 0 \end{matrix} & \begin{matrix} 0 & 0 \end{matrix} & \tilde{q}_\Omega T \end{bmatrix}. \tag{4}$$

In contrast to the CWNA model, the CT model is a nonlinear one if the turn rate Ω is not a known constant. In practice, the linear acceleration noise PSD levels in both dimensions are assumed to be equal; i.e., $\tilde{q}_\xi = \tilde{q}_\eta$. The general guidelines for selecting an appropriates levels of these noise parameters can be found in [1].

B. Sensor Measurement Model

A sensor collects measurements of the target range and azimuth angle according to the following measurement model [14]:

$$\mathbf{z} = \begin{bmatrix} r \\ a \end{bmatrix} = \begin{bmatrix} \sqrt{x^2 + y^2} \\ \tan^{-1}\left(\dfrac{y}{x}\right) \end{bmatrix} + \begin{bmatrix} w_r \\ w_a \end{bmatrix} \tag{5}$$

where w_r and w_a are independent zero mean Gaussian noises with standard deviations σ_r and σ_a, respectively. Note that this measurement has been normalized to the sensor's own known location.

C. Generating the State Estimates

1) Conversion of Measurements from Polar to Cartesian Coordinate: In practice the measurements are often reported in polar coordinates as in Eq. (5) with respect to the sensor location. Nevertheless, common motion models are given in Cartesian coordinates as shown earlier. Therefore, a sensor may need to first convert the polar measurements to Cartesian ones before generating its state estimates. A general unbiased conversion rule is given as follows [9]:

$$z_\xi^u = e^{\sigma_a^2/2} r \cos a \qquad z_\eta^u = e^{\sigma_a^2/2} r \sin a, \tag{6}$$

where σ_a is the standard deviation of the polar azimuth measurement.

[1] Note that a superscript T always denotes the transpose of a vector or matrix.

2) Filtering: The goal of a state estimator is to extract the state information $\mathbf{x}$ from measurement $\mathbf{z}$ that is corrupted by noise; this is done by running a filter that sequentially outputs the state estimate $\hat{\mathbf{x}}$ and its associated error covariance matrix $\mathbf{P}$. The Kalman filters (KFs) are linear minimum-mean-square-error (LMMSE)-optimal as the trace of $\mathbf{P}$ – characterizing the estimation error – at each step is minimized [12]. On the other hand, when the state dynamics and/or sensor measurement models are nonlinear, extended Kalman filters (EKFs) can be used to approximate the nonlinearity.

In many practical scenarios, the system characteristics can change over time. The interacting multiple model (IMM) serves a versatile tool for adapting the state estimation process in dynamic systems where a target can undergo different types of motion at different times. At any time, the system state is assumed to be in a number of possible modes that are described by their probabilities. The transition probabilities between modes from one estimation epoch to the next are assumed to follow a Markov chain. For each mode, the underlying filtering process is performed as described earlier, with the addition of evaluating the probabilities of different modes and interacting and mixing all the modes to generate an overall state estimate and error covariance [1].

D. Fusers

It is a well known fact that the common process noise results in correlation – described by the error cross-covariance – among estimates generated by multiple sensors. However, it is generally difficult to derive the exact cross-covariance terms in practice. We consider two types of fusers where the fused estimate can be obtained directly in closed forms with no cross-covariance calculation needed.

1) Track-to-Track Fuser without Cross-Covariance: In tracking applications, the track-to-track fuser (T2TF) is a linear fuser that is theoretically optimal in the linear minimum mean-square error (LMMSE) sense. In general, the fused state estimate $\hat{\mathbf{x}}_F$ and its error covariance $\mathbf{P}_F$ are defined for two sensors [1] as

$$\hat{\mathbf{x}}_F = \hat{\mathbf{x}}_1 + (\mathbf{P}_1 - \mathbf{P}_{12})(\mathbf{P}_1 + \mathbf{P}_2 - \mathbf{P}_{12} - \mathbf{P}_{21})^{-1}(\hat{\mathbf{x}}_2 - \hat{\mathbf{x}}_1) \tag{7}$$

$$\mathbf{P}_F = \mathbf{P}_1 - (\mathbf{P}_1 - \mathbf{P}_{12})(\mathbf{P}_1 + \mathbf{P}_2 - \mathbf{P}_{12} - \mathbf{P}_{21})^{-1}(\mathbf{P}_1 - \mathbf{P}_{21}) \tag{8}$$

where $\hat{\mathbf{x}}_i$ and $\mathbf{P}_i$ are the state estimate and error covariance from sensor i, respectively, and $\mathbf{P}_{ij} = \mathbf{P}_{ji}^T$ is the error cross-covariance between sensors i and j. However, when the sensor errors are correlated and the cross-covariance is unavailable, one may assume that the cross-covariance is zero in order to apply this linear fuser, even though the result will be suboptimal. The fuser would then be reduced to a simple convex combination of the state estimates:

$$\mathbf{P}_F = (\mathbf{P}_1^{-1} + \mathbf{P}_2^{-1})^{-1} \tag{9}$$

$$\hat{\mathbf{x}}_F = \mathbf{P}_F(\mathbf{P}_1^{-1}\hat{\mathbf{x}}_1 + \mathbf{P}_2^{-1}\hat{\mathbf{x}}_2) \tag{10}$$

2) Fast Covariance Intersection (CI) Algorithm: Another sensor fusion method is the covariance intersection (CI) algorithm. The intuition behind this approach comes from a geometric interpretation of the problem. If one were to plot the covariance ellipses for $\mathbf{P}_F$ (defined as the locus of points $\{\mathbf{y} : \mathbf{y}^T\mathbf{P}_F^{-1}\mathbf{y} = c\}$ where c is some constant), the ellipses of $\mathbf{P}_F$ are found to always contain the intersection of the ellipses for $\mathbf{P}_1$ and $\mathbf{P}_2$ for all possible choices of $\mathbf{P}_{12}$ [3]. The intersection is characterized by the convex combination of sensor covariances:

$$\mathbf{P}_F = (\omega_1\mathbf{P}_1^{-1} + \omega_2\mathbf{P}_2^{-1})^{-1} \tag{11}$$

$$\hat{\mathbf{x}}_F = \mathbf{P}_F\left(\omega_1\mathbf{P}_1^{-1}\hat{\mathbf{x}}_1 + \omega_2\mathbf{P}_2^{-1}\hat{\mathbf{x}}_2\right), \quad \omega_1 + \omega_2 = 1 \tag{12}$$

where $\omega_1, \omega_2 > 0$ are weights to be determined (e.g., by minimizing the determinant of $\mathbf{P}_F$).

A fast CI algorithm has been proposed in [13] where the weights are found based on an information-theoretic criterion so that ω_1 and ω_2 can be solved for analytically as follows:

$$\omega_1 = \frac{D(p_1, p_2)}{D(p_1, p_2) + D(p_2, p_1)} \tag{13}$$

where $D(p_A, p_B)$ is the Kullback-Leibler (KL) divergence from $p_A(\cdot)$ to $p_B(\cdot)$, and $\omega_2 = 1 - \omega_1$. When the underlying estimates are Gaussian, the KL divergence can be computed as

$$D(p_i, p_j) = \frac{1}{2}\left[\ln\frac{|\mathbf{P}_j|}{|\mathbf{P}_i|} + \mathbf{d}_X^T\mathbf{P}_j^{-1}\mathbf{d}_X + Tr(\mathbf{P}_i\mathbf{P}_j^{-1}) - k\right], \tag{14}$$

where $\mathbf{d}_X = \hat{\mathbf{x}}_i - \hat{\mathbf{x}}_j$, k is the dimensionality of $\hat{\mathbf{x}}_i$, and $|\cdot|$ denotes the determinant. This fast-CI algorithm will be used for a quantitative comparison against the above T2TF with unavailable cross-covariances.

E. Target Trajectory

The initial state of the target in Cartesian coordinates (with the position in meters and velocity in m/s) is set to be [14] $\mathbf{x}(0) = [x(0) \;\; \dot{x}(0) \;\; y(0) \;\; \dot{y}(0)]^T = [0 \;\; 0 \;\; 20000 \;\; 250]^T$. At $t = 60$ s, the test target starts to take a left turn at a turn rate of 2°/s for 30 s, and then continues straight until $t = 150$ s. The sampling rate of the sensors is once every two seconds, i.e., $T = 2$ s. During the straight-line movement, the process noise power spectral densities $\tilde{q}_\xi = \tilde{q}_\eta = 0.0018 \text{ m}^2/\text{s}^3$; during the turn, on the other hand, $\tilde{q}_\xi = \tilde{q}_\eta = 32 \text{ m}^2/\text{s}^3$ and $\tilde{q}_\Omega = 5 \times 10^{-7} \text{ m}^2/\text{s}^3$ [14].

In what follows, we investigate tracking of this target with individual sensors running KF and IMM respectively, and with both sensors. In particular, we are interested in (1) the actual error performance, and (2) how the theoretical error, as described by the error covariance matrix, differs from the actual estimation error, under variable communication and computation constraints.

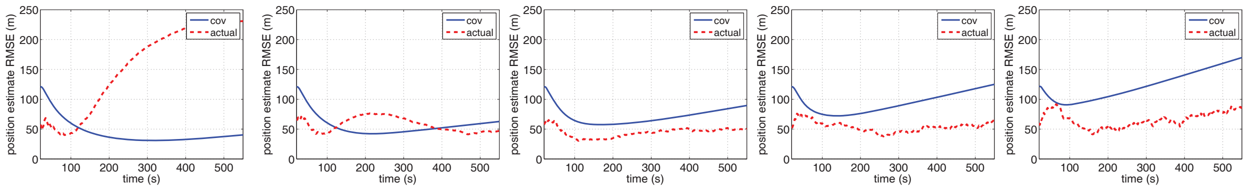

(a) 0.01 (b) 0.1 (c) 1 (d) 10 (e) 100

Fig. 1: Theoretical (covariance-based "cov") and actual position estimate root-mean-square-error (RMSE) performance with a hypothetical extended straight line movement over time. The numbers indicate the multiples of the exact process noise power spectral density (PSD) in Eq. (2).

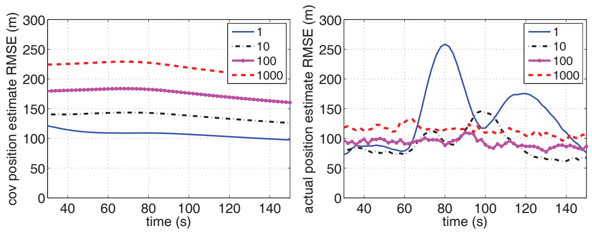

(a) (b)

Fig. 2: Position estimate RMSE performance of the maneuvering target tracking with Kalman filters of different levels of noise power spectral density (PSD) $\tilde{q}$ (unit: $\mathrm{m}^2/\mathrm{s}^3$): (1) theoretical; (2) actual

III. Estimation and Consistency Performance of Individual Sensors

We first look at the estimation performance of individual sensors – before the estimates are communicated to the fusion center – along with the consistency performance of the filters run.

A. Kalman Filter

A Kalman filter, under certain settings, such as perfectly matched process noise (to the actual underlying system model) along with linear process and measurement models, generates a stream of state estimates, whose mean-square error (MSE) at any time epoch always matches the error derived from the corresponding error covariance matrix [6]. However, note that the measurement conversion process in Eq. (6) is a nonlinear one, and this consistency may no longer hold. To verify this, we modified the original trajectory so that the straight-line movement alone now lasts 9 minutes. Fig. 1(c) shows the theoretical ("cov") and actual position root-mean-square error (RMSE) performance with perfectly matched process noise PSD levels. The mismatch between the two curves stems partly from the nonlinearity of the measurement conversion step, but also reflects the important fact that KFs aim to minimize the trace of the covariance error matrix, in this case, the sum of all squared position and velocity error components. Here we are mainly interested in a portion of the sum, namely, the position estimation error performance. In addition, the root square operation is also nonlinear, further contributing to the discrepancy between the two curves.

In practice, a KF may run using a process noise PSD that is different from the level that best approximates the actual target movement. Filter divergence [12] can occur, resulting in elevated estimation error overtime. Fig. 1 displays how the KF with variable process noise levels – from 1/100th of the actual $\tilde{q}$ to 100 times – performs under the same condition. From the plots, filter divergence can easily occur when the presumed noise level is far below the true level (as in (a)), whereas a too conservative noise level used for filtering (as in (e)) can lead to overall elevated estimation errors. Meanwhile, the theoretical, or covariance-based errors, seem to only slightly change according to the changes in the presumed noise level. This demonstrates that it is desirable, at least in this situation, that the process noise level used for filtering is as close to the actual scenario as possible. Compared to other cases, despite the discrepancy between the two curves in (c), the "cov" errors are within a factor between 1.3 and 1.6 as against the actual errors, the most stable among all.

However, if this "matched" noise level (to the straight-line movement) were to be used by the filter through the entirety of the original trajectory, the error would soon diverge as the maneuver starts. In fact, from Fig. 2, it would take roughly 10,000 times the process noise level to yield decent performance to accommodate the extent of noise elevation for the turn phase. More specifically, compared to lower presumed process noise (such as 1 $\mathrm{m}^2/\mathrm{s}^3$ and to a lesser extent, 10 $\mathrm{m}^2/\mathrm{s}^3$), where the errors during/after the turn are high and unstable, as well as higher presumed process noise (such as 1,000 $\mathrm{m}^2/\mathrm{s}^3$), where the overall errors start to become unnecessarily high, a level at 100 $\mathrm{m}^2/\mathrm{s}^3$ seems to be able to balance the needs of stabilizing and reducing the peak error performance during and after the maneuver as well as maintaining a decent tracking performance during straight-line segments. In the following, this noise level will be set for the sensor running KF. In the meantime, from Fig. 2(a), the theoretical curves seem to follow a simple relationship (that is more often not a good representation of the actual error performance); at the above set level, the theoretical position RMSE values are within a factor of two compared to the actual errors.

B. IMM Filter

The complexity of IMM filters is not only reflected in the choice of process noise levels, but also the individual modes that can cover multiple motion trajectory types. Here we consider a two-mode IMM comprising a KF and an EKF (used to describe the possible straight-line and turn movements

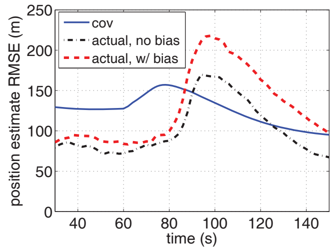

Fig. 3: Position estimate RMSE performance of the maneuvering target tracking with an IMM filter

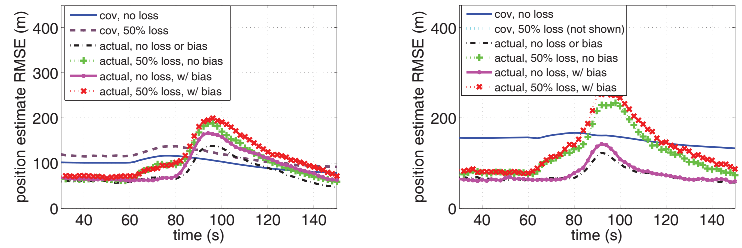

(a) (b)

Fig. 4: Fused position estimate RMSE performance of the maneuvering target tracking with (a) track to track fuser (T2TF); (b) fast covariance intersection (CI) fuser

respectively), whose process noise levels are matched to those in the CWNA and CT models in Sec. II respectively.

From Fig. 3, during the initial straight-line motion stage, the IMM estimator yields somewhat more accurate estimates compared to the KF estimator, thanks to the better match of the process noise level; however, after the turn begins at $t = 60$ s, its error gradually increases and at around $t = 80$ s, shoots up rapidly till shortly after the maneuver ends at $t = 90$ s. Afterward, the error decreases, much less precipitately compared to the previous phase, and does not fall back to the pre-maneuver level until around $t = 140$ s. This observation reflects the fact that a mode "switch" – in terms of the probability changes for individual modes – occurs gradually and thus usually lags that of the actual underlying motion change. Interestingly, the curve for the theoretical error shows that it changes more readily with the actual motion change, e.g., at $t = 60$ s, although the end of the maneuver at $t = 90$ s doesn't seem to affect its downward trend after the peak reached earlier.

Next, a positive bias term is added to the measurement of the IMM estimator, where the bias values are $\sigma_r/\sqrt{5}$ for the range and $\sigma_a/\sqrt{20}$ for the azimuth. Also from Fig. 3, the tracking errors with this added bias seem to much elevated, especially during and after the maneuver. However, the theoretical curve remains the same, which means the sensor itself is oblivious to the fact that its measurements are biased.

IV. Estimation and Consistency Performance with Two-Sensor Fusion

We explore the estimation and consistency performance for the maneuver target tracking with both the track-to-track fuser (T2TF) and fast-CI fusers – combining the IMM filter (Sensor 1) and KF (Sensor 2) outputs as described in the previous section – under varying conditions.

A. Performance with T2TF

From the plots in Fig. 4(a), the following can be observed for the fused estimates using T2TF under the condition that there is no communication constraints (e.g., loss or delay) or computation constraints (e.g., sensor bias). First, fusion can effectively reduce the estimation error in both straight-line and turn phases of the trajectory. For instance, the peak RMSE error towards the end of the turn can be reduced by nearly 20% from that of the IMM filter alone (although this error is still higher than that of the KF filter with a steady process noise set at 100 $\mathrm{m}^2/\mathrm{s}^3$); and for the most part of the straight-line segments, the estimation errors appear better than in the cases using individual filters. In addition, the shape and trend of the curve largely resemble those of the IMM filter, thanks to the relatively stable performance of the KF. When the same measurement bias term (as in the previous section) is added to the IMM filter, a similarly trending curve is seen from the plot. In the meantime, the theoretical curves prior to and after adding in measurement bias are identical for the same reason as described in the IMM case.

The communication constraints are determined by the long-haul link conditions. For now, we consider a 50% communication loss rate encountered over the links from both sensors to the fusion center. Loss can effectively reduce the number of estimates that are successfully received by the fusion center. If the fusion center applies prediction from the previously available estimates for any sensor, then a fused estimate at time k could be obtained from (1) available $\hat{\mathbf{x}}_1$ and $\hat{\mathbf{x}}_2$ at k; (2) available $\hat{\mathbf{x}}_1$ but a predicted estimate from an earlier time for Sensor 2; (3) available $\hat{\mathbf{x}}_2$ but a predicted estimate from an earlier time for Sensor 1; and (4) predicted estimates from (possibly different) earlier times for both sensors. Prediction generally introduces more uncertainty and higher errors, which can be confirmed from the plot in Fig. 4(a), where under 50% loss, the position RMSE seems to be much higher during and shortly after the maneuver (also higher than the case with bias alone at the specified level). The curve with both loss and bias is also plotted, whose main difference from the loss-only case is largely seen during the straight-line segments. Finally, the theoretical curve (regardless of bias) with the loss case has nearly the same shape and trend as that without loss.

Usually, the T2TF is considered an "optimistic" fuser, meaning the actual error is typically worse than the theoretical error indicated by the covariance matrix [1]. The "pessimistic" behavior observed here, i.e., the worse theoretical error outside the "peak" segment, is due largely to the same pattern at both the IMM and KF. In other words, the optimistic fuser can't offset the strong pessimistic characteristic of the individual components.

B. Performance with Fast-CI

The estimation and fusion performance under the same set of conditions is studied for the fast-CI fuser. From the plots in Fig. 4(b), in contrast to the T2TF case, in lossless scenarios, the tracking error doesn't noticeably increase until $t = 75$ s; and after peaking out near the end of the maneuver at $t = 90$ s, it falls back at the same rate and returns to that of the pre-maneuver level at around $t = 120$ s. Also the peak errors for both bias and non-bias cases are also noticeably lower than their T2TF-fused counterparts. Meanwhile, from the theoretical curve, the error in the straight-line case is already so high that any change when the turn is initiated is barely noticeable. This can be described by the pessimistic nature of the CI fuser, where the covariance-indicated error is typically worse off than the actual error. The entirety of the trajectory is characterized by higher theoretical error, more so for the segments away from the peak near the center.

Next, a 50% loss rate is again imposed onto the system. Much elevated errors are observed for both bias and non-bias cases; in fact, the errors are in general 20%-30% higher even compared to the corresponding T2TF-fused values. This can be explained by the geometric interpretation of the CI-based fusers. Since the fusion result is described by an ellipse that contains the intersection of the two ellipses corresponding to errors of both sensors, with increasing loss, more prediction steps need to be performed, corresponding to the area increase of individual ellipses; as a result, to contain both growing ellipses (often in different directions), the CI fuser must come up with an even bigger ellipse, representing a much higher error. Also due to the very pessimistic nature of the CI fusers, the theoretical measure grows even faster, sometimes so fast as to reach a unreasonably high level and overall experience instability based on the instantaneous loss conditions; this is the reason why the theoretical curve for the lossy case is not shown in Fig. 4(b) at all.

To sum up the differences in estimation and consistency performances using T2TF and fast-CI fusers, under lossless conditions, the fast-CI fuser is able to recover faster from the effect of motion change and doesn't have as high a peak error as in the T2TF case; however, the loss can severely limit this advantage, resulting in much elevated tracking errors. The optimistic nature of the T2TF serves to offset the effect of pessimistic individual filters, whereas the opposite feature of the fast-CI fuser serves to reinforce it. In addition, under loss conditions, the theoretical performance of the fast-CI fuser, a poor indicator of the actual errors, can become highly unstable.

V. Estimation and Consistency Performance with Information Feedback

Usually the information flow in the estimation and fusion applications is from sensors to the fusion center only. The main purpose of information feedback from the fusion center to the sensors is to combat any biases at the individual sensors [5]. In Fig. 5, feedback is sent back to Sensor 1 (as the IMM filter in this work) that is unaware of its measurement bias, in the hope that the extra tracking error can be somewhat alleviated. In what follows, we first analyze the timing issues in information feedback, and then we evaluate the tracking accuracy and consistency performances using T2TF and CI fusers with information feedback.

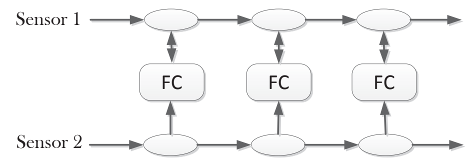

Fig. 5: Feedback from the fusion center to the biased Sensor 1

A. Analysis of Feedback Timing

Over a lossy long-haul communication link, any feedback message is also subject to loss on the reverse link; in other words, a feedback message may never be received by the intended sensor at all. However, in what follows, we mainly examine how the communication delay and timing of the feedback schedules also affects the information exchange.

The latency that a message undergoes before arriving at the destination may consist of the initial detection and measurement delay, data processing delay, propagation delay, and transmission delay, among others. For ease of analysis, suppose $f_F(\cdot)$ and $f_R(\cdot)$ represent the forward and reverse link delay pdf's describing a shifted exponential distribution:

$$f_F(t) = \frac{1}{\mu_F}\exp^{-\frac{t-T_I}{\mu_F}},\ f_R(t) = \frac{1}{\mu_R}\exp^{-\frac{t-T_I}{\mu_R}},\ \text{for } t \geq T_I, \tag{15}$$

where T_I serves as the common link and processing delay, or the minimum delay any message must experience, and μ's are the mean of the random delay beyond T_I that can be affected by factors such as weather and terrain. Then the pdf $h(\cdot)$ of the total time for a feedback message to return to a sensor (starting from the time when the estimate was originally sent out by the sensor to the fusion center) can be found as

$$\begin{aligned} h(t) &= \frac{1}{\mu_F - \mu_R}\left(e^{-\frac{t-2T_I}{\mu_F}} - e^{-\frac{t-2T_I}{\mu_R}}\right) \\ &= \frac{\mu_F}{\mu_F - \mu_R}e^{\frac{T_I}{\mu_F}}f_F(t) - \frac{\mu_R}{\mu_F - \mu_R}e^{\frac{T_I}{\mu_R}}f_R(t), \\ &\qquad \text{for } t \geq 2T_I, \end{aligned} \tag{16}$$

and the distribution function can be found by replacing $f_F(\cdot)$ and $f_R(\cdot)$ with their respective cdf's respectively. With this distribution, the probability mass function (pmf) of the time when a subsequently updated estimate is sent out by the sensor can be obtained by taking the ceiling of t, and in turn the pdf of the time when the updated message takes effect at the fusion center by superimposing the above time on another forward-link communication delay.

In our two-sensor case, it can be derived that in a lossless scenario, an average amount of $\mathbb{E}[\max(T_1, T_2)] = T_I + 3\mu_F/2$ time is needed before the fusion center receives both sensor estimates. However, if the fusion center restricts the fusion time to within a certain range, the total amount of time it takes for the feedback message to arrive can be found to follow the distribution

$$\Pr\{t \leq D\} = \iint_0^D f_R(t|T_F) g(T_F) \mathrm{d}t \mathrm{d}T_F, \tag{17}$$

where $f_R(t|T_F)$ is the conditional pdf contingent on a certain T_F value, and $g(\cdot)$ is the prior pdf of the fusion/feedback time. If the fusion time is chosen uniformly from the interval $[T_I, D-T_I]$ (accounting for the propagation delay), i.e., $g(T_F) = 1/(D-2T_I)$ for $T_F \in [T_I, D-T_I]$ and 0 otherwise, then the distribution in Eq. (17) can be further derived as

$$\begin{aligned} \Pr\{t \leq D\} &= \frac{1}{D-2T_I} \int_{T_I}^{D-T_I} (1 - e^{-\frac{D-T_I-t}{\mu_R}}) \mathrm{d}t \\ &= 1 - \frac{\mu_R}{D-2T_I} F_R(D-T_I), \end{aligned} \tag{18}$$

which is a further improvement compared to the distribution derived with Eq. (16) alone, i.e., without the additional prior knowledge about T_F.

Generally, the average amount of time it takes for the feedback message to arrive is $T_I + \mu_R$; with the initial period T_F, the total average latency between the time when the feedback message is received and the (prior) time instant the message describes is

$$T_F + T_I + \mu_R \leq 2T_I + 3\mu_F/2 + \mu_R. \tag{19}$$

If this duration exceeds the estimation interval T, the sensor has already generated a new estimate before the feedback message arrives; then it would have to either use prediction or measurements to project this delayed fused estimate to its next pending estimate [5], with an average of no less than $\lceil \frac{2T_I+3\mu_F/2+\mu_R}{T} \rceil$ prediction steps, or alternatively, using each measurement $\lceil \frac{2T_I+3\mu_F/2+\mu_R}{T} \rceil$ times, both of which could potentially offset the very benefit of bias reduction.

To summarize, to reduce the potential negative effect of estimation error increase due to prediction and/or measurement bias following delayed feedback, it is preferable to use a smaller T_F. However, with an early time cutoff, the fusion center is using less information for fusion, which may have a more adverse effect on tracking performance as a decrease in T_F can easily reduce the probability of having new arrivals from both sensors.

B. Performance with Feedback

Next we investigate the tracking performance with feedback sent back to the IMM filter whose measurement bias profile has been used in both Secs. III and IV. The different time parameters are listed in Table I.

TABLE I: Time parameters

parameters	T_I	μ_F	μ_R	D	D_F
values (s)	0.5	0.3	0.2	2	1.5

1) Fast-CI: Time constraints essentially have the same effect as communication loss to CI-based fusers: the probability that a message is successfully delivered to the destination by a certain time is reduced. In Fig. 6(a), without feedback, the error performance with communication delay as specified earlier can be seen. Of note is the unstable theoretical curve due to the pessimistic nature of the fuser and much elevated errors with unavailable tracks.

As feedback depends on timely communication of the messages involved, an early time cutoff would serve to reduce the effective number of messages to received by the deadline. By comparing Figs. 6(b), where $D = 2$ s and D_F = 1.5 s, with 6(c), where $D = 1.2$ s and D_F = 0.8 s, we observe that the gain from feedback in the former case (from the baseline no-feedback case) is reduced in the latter; whereas the estimation errors are noticeably lower with a less stringent deadline, early time cutoff renders the CI output largely the same as compared to the no-feedback case. The one less step for prediction or measurement update (after the feedback message arrives) seems not sufficient to offset the fusion gain lost by setting an earlier cutoff. Interestingly, the theoretical error curve appears to be pulled down with a tighter schedule. Finally, in Fig. 6(d), the feedback performance with the original schedule but under a 50% loss rate is plotted. Sending back fused states that are highly erroneous in the first place doesn't help: The resulting errors are worse than without feedback, even much higher than those of individual filters; and as in the lossy case without feedback, the theoretical curve again is highly unstable with very large values.

2) T2TF: We run the same set of feedback schedules with variable loss conditions on the T2TF. Apparently, compared to the curves in Fig. 4(a), the feedback messages are able to largely reshape the error curves of Sensor 1 (IMM) – and in turn, of the fused estimates – around the maneuver period. In particular, from Fig. 7, the peaks of the error bell curves are significantly narrowed by the feedback, although the peaks seem to largely retain their no-feedback values. Another prominent characteristic of the T2TF curves, in contrast to their CI counterparts, is that the errors – theoretical or actual – are much more stable with variations in time cutoffs/schedules and loss rates. An increasing loss rate seems to elevate and widen the peak of the fused state error curves, so does a reduced cutoff time for fusion and feedback. Besides, as more communication and computation constraints are imposed, feedback seems to "homogenize" the IMM and fused estimate curves: whereas the two are far apart in (a), they move closer with increasing loss and/or time constraints, and almost overlap toward the post-maneuver segment in (d).

In summary, while it's generally beneficial to feed the fused state information back to the biased sensors, communication loss/delay as well as fusion and feedback schedules can limit the potential gain from feedback. Whereas with feedback, the fast-CI fuser performs well in lossless conditions compared to the T2TF, it is more sensitive to the above constraints, resulting in elevated and unstable tracking performance. In addition, covariance-based error measures are sometimes a

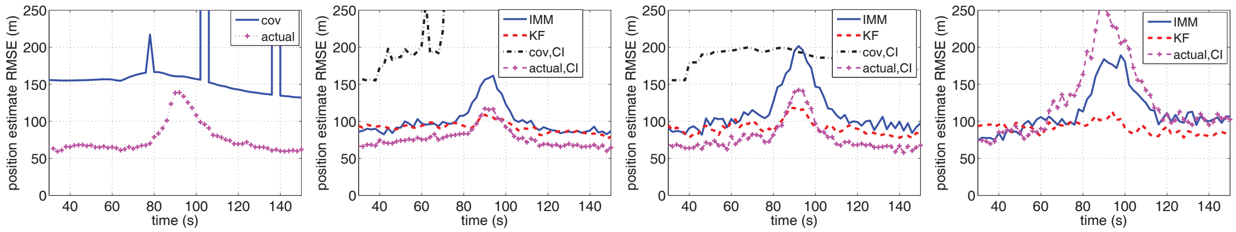

(a) (b) (c) (d)

Fig. 6: Position estimate RMSE performance of the maneuvering target tracking with the fast-CI fuser and biased estimates from the IMM filter: (a) the theoretical performance ("cov") can easily become unstable with increasing communication constraints, i.e., higher loss and/or tighter reporting deadline; (b) with feedback, no loss; (c) with feedback, reduced reporting deadline, no loss; (d) with feedback, 50% loss ("cov" not shown)

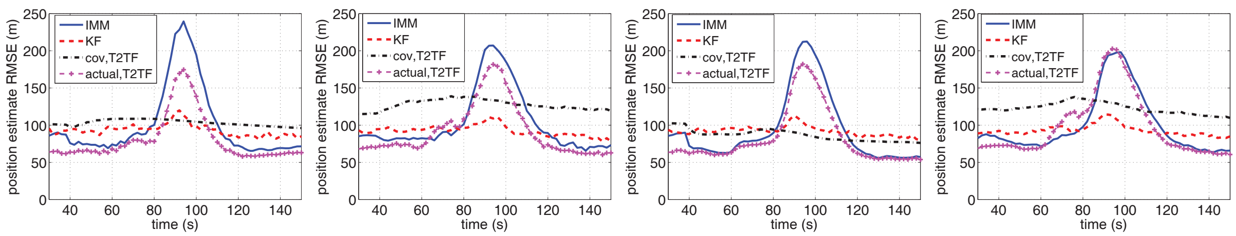

(a) (b) (c) (d)

Fig. 7: Fused position estimate RMSE performance of the maneuvering target tracking with the T2TF and feedback: (a) no loss; (b) 50% loss; and with tighter reporting and feedback time constraints in (c) no loss; (d) 50% loss

poor representation of the actual error performance and should be used with caution.

VI. Conclusion

In this work, we have investigated estimation and fusion accuracy and consistency performances using a maneuver target tracking example. In particular, the effects of a number of communication and computation constraints, including loss/delay, sensor bias, as well as fusion and feedback time cutoffs, over a long-haul sensor network have been studied. Since in practice, the fusion center may need to rely on the expected information quality from individual sensors to make its decisions [6], of future interest are ways to adaptively incorporate the inconsistent error measures in a complex dynamic system, based on the short- and long-term objectives of sensor fusion. Extensions of this work also include studies of information quality and consistency performance for other error measures other than MSE/RMSE.

References

[1] Y. Bar-Shalom, P. K. Willett, and X. Tian. *Tracking and Data Fusion: A Handbook of Algorithms*. YBS Publishing, 2011.

[2] A. Chiuso and L. Schenato. Information fusion strategies and performance bounds in packet-drop networks. *Automatica*, 47:1304–1316, Jul. 2011.

[3] S. J. Julier and J. K. Uhlmann. *General Decentralized Data Fusion with Covariance Intersection, ser. Handbook of Multisensor Data Fusion*. CRC Press, 2001.

[4] Q. Liu, X. Wang, and N. S. V. Rao. Staggered scheduling of estimation and fusion in long-haul sensor networks. In *Proc. 16th International Conference on Information Fusion (FUSION 2013)*, pages 1699–1706, Istanbul, Turkey, Jul. 2013.

[5] Q. Liu, X. Wang, and N. S. V. Rao. Information feedback for estimation and fusion in long-haul sensor networks. In *Proc. Information Fusion (FUSION), 2014 17th International Conference on*, Salamanca, Spain, Jul. 2014.

[6] Q. Liu, X. Wang, and N. S. V. Rao. Fusion of state estimates over long-haul sensor networks with random loss and delay. *IEEE/ACM Transactions on Networking*, 2015.

[7] Q. Liu, X. Wang, N. S. V. Rao, K. Brigham, and B. V. K. Vijaya Kumar. Performance of state estimate fusion in long-haul sensor networks with message retransmission. In *Proc. Information Fusion (FUSION), 2012 15th International Conference on*, pages 719–726, Singapore, Singapore, Jul. 2012.

[8] M. Mallick and K. Zhang. Optimal multiple-lag out-of-sequence measurement algorithm based on generalized smoothing framework. In *Proc. SPIE, Signal and Data Processing of Small Targets*, San Diego, CA, Apr. 2005.

[9] L. Mo, X. Song, Y. Zhou, Z. Sun, and Y. Bar-Shalom. Unbiased converted measurements for tracking. *Aerospace and Electronic Systems, IEEE Transactions on*, 34(3):1023–1027, Jul. 1998.

[10] N. S. V. Rao, K. Brigham, B. V. K. Vijaya Kumar, Q. Liu, and X. Wang. Effects of computing and communications on state fusion over long-haul sensor networks. In *Proc. Information Fusion (FUSION), 2012 15th International Conference on*, pages 1570–1577, Singapore, Singapore, Jul. 2012.

[11] E. I. Silva and M. A. Solis. An alternative look at the constant-gain kalman filter for state estimation over erasure channels. *Automatic Control, IEEE Transactions on*, 58(12):3259–3265, Dec. 2013.

[12] D. Simon. *Optimal state estimation: Kalman, H [infinity] and nonlinear approaches*. Wiley-Interscience, 2006.

[13] Y. Wang and X. Li. Distributed estimation fusion with unavailable cross-correlation. *Aerospace and Electronic Systems, IEEE Transactions on*, 48(1):259–278, Jan. 2012.

[14] T. Yuan, Y. Bar-Shalom, and X. Tian. Heterogeneous track-to-track fusion. In *Information Fusion (FUSION), 14th International Conference on*, pages 1–8, Jul. 2011.

[15] S. Zhang and Y. Bar-Shalom. Optimal update with multiple out-of-sequence measurements with arbitrary arriving order. *Aerospace and Electronic Systems, IEEE Transactions on*, 48(4):3116–3132, Oct. 2012.